Murphy’s Tank

Automatic Gap-Crossing Vehicle

Design and Manufacturing Final Report

ME 2500J - Summer 2026

Malcolm Von, Apeel Subedi, Andrew Grosso, and Dhruv Jha

Shanghai Jiao Tong University

Shanghai 200240, People’s Republic of China

Group 5

August 5, 2026

Abstract

Murphy's Tank is an automatic timed tracked vehicle developed to cross a 200 mm table gap while prioritising structural strength and load capacity. The initial six-wheel arrangement tipped when its front wheels lost support, so a continuous-tread system was added to maintain reactions on both tables. The final prototype completed one of two official trials, giving a 50 % success rate. During the successful trial, the front wheels traversed the 200 mm gap and the complete vehicle passed the finish line in approximately 6 s. A separate flat-floor test showed that the vehicle could move while carrying a 75 kg person, above the 40 kg minimum payload objective. Quasi-static analysis explains the original tipping mechanism, while frame finite element analysis supports the selection of printed PLA with local sheet-steel reinforcement. The principal reliability limitations were tread derailment and transmission-belt slip caused by the absence of adjustable tensioners.

Contents

Nomenclature

Symbol	Definition	Unit
G	Width of the table gap	m
s	Centre-to-centre spacing between consecutive wheel pairs	m
Δ	Difference between gap width and wheel spacing, $G - s$	m
m	Total vehicle or payload mass	kg
g	Gravitational acceleration	m/s^2
N_F, N_M, N_R	Front-, middle-, and rear-wheel normal reactions	N
e	Horizontal offset of the centre of mass from the middle-wheel contact	m
M_{tip}	Gravitational tipping moment about the middle-wheel contact	N m
$N_{\text{near}}, N_{\text{far}}$	Resultant track reactions from the near and far tables	N
$x_{\text{near}}, x_{\text{far}}$	Centres of pressure of the near- and far-table track contacts	m
x_C	Horizontal position of the vehicle centre of mass	m
W	Weight or applied vertical load	N
F	Applied force	N
δ_{max}	Maximum resultant displacement	mm
k_{eff}	Effective vertical stiffness	N/mm
$\sigma_{\text{vM,max}}$	Maximum von Mises stress	MPa
ε_{max}	Maximum equivalent strain	–
σ_{ref}	Reference printed-PLA yield strength used for the nominal factor of safety	MPa
FoS_{nom}	Nominal factor of safety, $\sigma_{\text{ref}}/\sigma_{\text{vM,max}}$	–
T_{motor}	Rated gearbox-output torque of one motor	N m
T_{total}	Combined rated torque at the two driven axles	N m

Symbol	Definition	Unit
n_{axle}	Axle rotational speed	rpm
d	Wheel diameter	m
r	Wheel radius	m
v_{nom}	Nominal kinematic vehicle-speed estimate	m/s
v_{course}	Average speed over the official course	m/s
L_{run}	Minimum travel distance for the complete official run	m
F_{drive}	Ideal circumferential driving force	N
P	Electrical power	W
V	Voltage	V
I	Electric current	A
E	Stored electrical energy	W h
t	Time	s or h

I Introduction

Unmanned ground vehicles can transport equipment without requiring a person to enter the working area. In this project, Group 5 was tasked with designing and manufacturing an automatic vehicle that could cross a gap of at least 200 mm between two tables. The vehicle had to begin behind a start line located 200 mm before the gap and move completely beyond an end line located 200 mm after the gap. No physical assistance or flight was allowed once the vehicle started moving. The preferred initial and final vehicle envelope was 500 mm by 300 mm by 300 mm, as specified in the project brief [1].

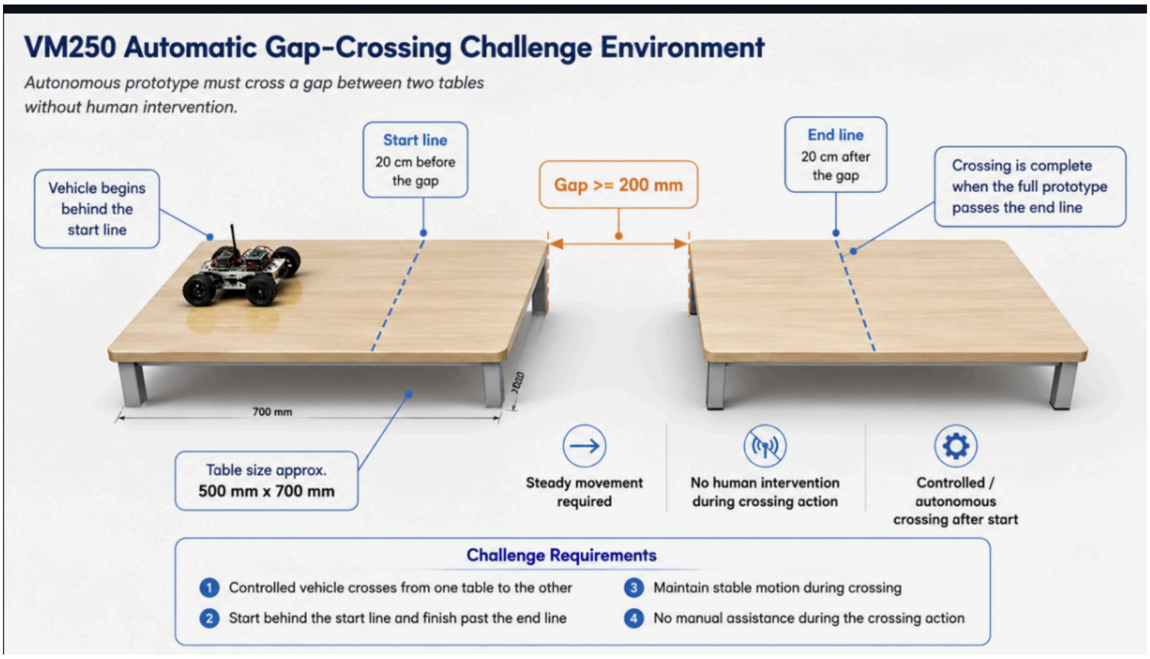

Figure 1: Automatic gap-crossing challenge environment and main task requirements.

Our vehicle, Murphy's Tank, was designed mainly for load capacity and structural strength rather than maximum speed. It used two 12 V DC gearmotors, timing belts, six wheels, three steel shafts, journal bearings, and a modular PLA frame reinforced with formed steel sheet. The first prototype used six separate wheels, but testing showed that it tipped when the front wheels lost contact with the table. Continuous treads were later added to maintain support during the crossing.

The final tracked prototype completed one of two official trials, corresponding to a 50 % success rate. In the successful run, the front wheels traversed the 200 mm gap and the entire vehicle passed the official finish line in approximately 6 s. The frame also carried a 75 kg person on a level floor without visible damage. Finite element analysis under a 1000 N stretch load predicted a maximum displacement of 0.097 67 mm. The main reliability problem was tread derailment, which showed that tread alignment and tension required further improvement.

II Product Design

A Problem Definition

The product was designed to move its own weight, and ideally an additional payload, across a gap between two tables. The design therefore needed enough motor torque to move forward and enough stability to prevent tipping while the wheel or tread contact points changed.

The main task constraints were taken from the project brief [1]:

- cross a gap of at least 200 mm;
- begin 200 mm before the gap;
- finish completely beyond a line 200 mm after the gap;
- move without human assistance after starting;
- remain stable throughout the crossing;
- avoid flying or jumping over the gap; and
- fit within the preferred 500 mm by 300 mm by 300 mm envelope at the start and finish.

1 Customer Requirements

The customer requirements were based on the challenge rules and the expected performance of the vehicle:

- fit within the preferred starting and finishing envelope;
- cross the 200 mm gap automatically;

- remain stable while carrying a load;
- prevent tipping during support transfer;
- operate automatically after starting;
- be easy to start and control;
- remain lightweight where possible;
- be durable and reliable;
- have a reasonable prototype cost;
- operate safely;
- cross the gap within a short time; and
- be simple to manufacture and assemble.

2 Engineering Specifications

The customer requirements were converted into measurable engineering specifications:

- vehicle volume at the start and finish;
- overall wheelbase or tread length;
- wheel spacing and support width;
- acceleration smoothness;
- total vehicle mass;
- motor power and output torque;
- battery capacity;
- prototype cost;
- timed run duration; and

- maximum travelling speed.

The minimum payload objective was 40 kg. A 100 kg load was treated as a stretch goal for structural analysis rather than as a required specification, while the completed prototype was physically tested with a 75 kg payload on a level surface. The vehicle was therefore designed around a high-load objective, so structural strength, support width, motor torque, and stability were given greater importance than maximum speed.

3 Quality Function Deployment

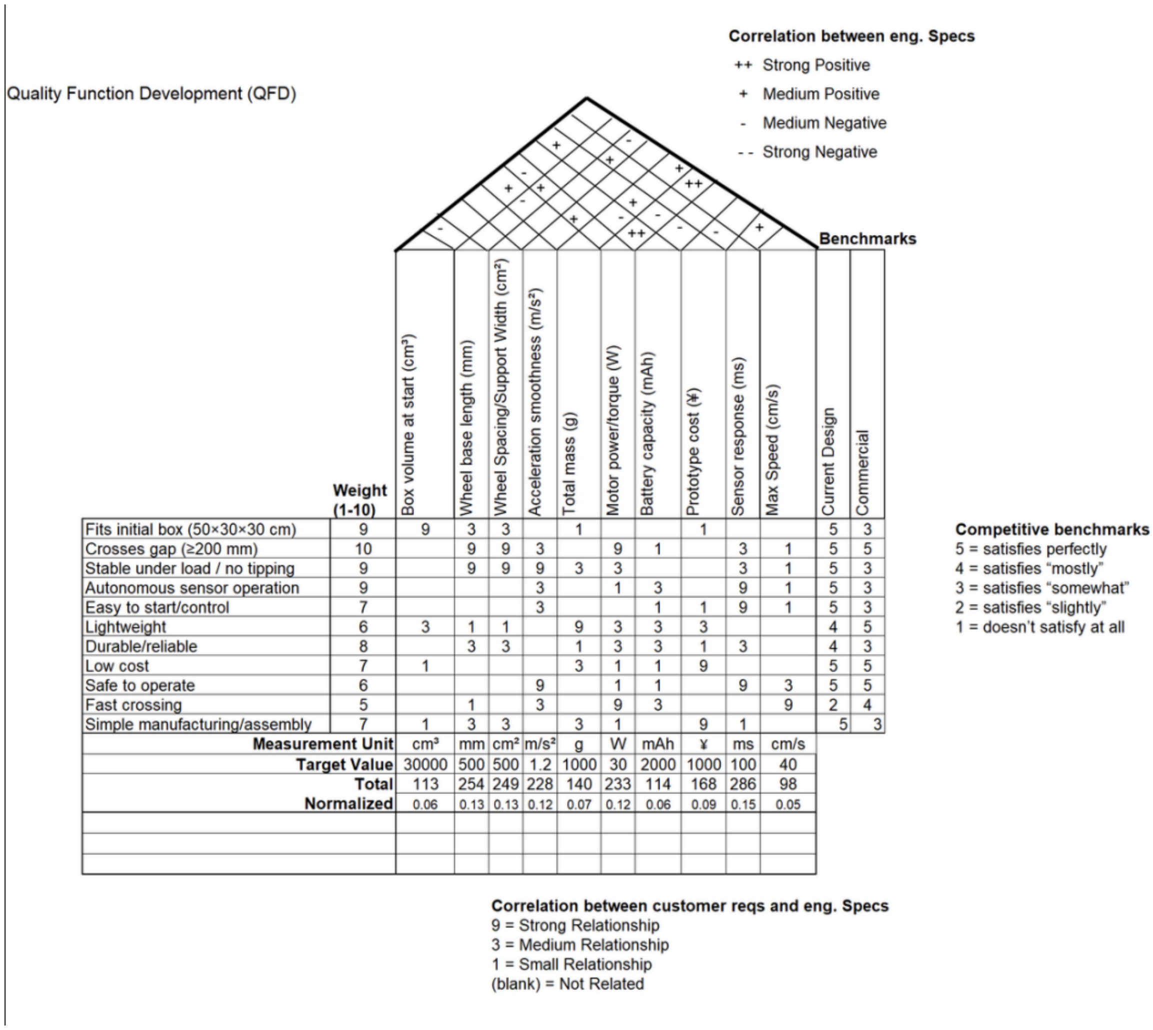

	Weight (1-10)	Box volume at start (cm³)	Wheel base length (mm)	Wheel Spacing/Support Width (cm²)	Acceleration smoothness (m/s²)	Total mass (g)	Motor power/torque (W)	Battery capacity (mAh)	Prototype cost (¥)	Sensor response (ms)	Max Speed (cm/s)	Current Design	Commercial
Fits initial box (50×30×30 cm)	9	9	3	3		1			1			5	3
Crosses gap (≥200 mm)	10		9	9	3		9	1		3	1	5	5
Stable under load / no tipping	9		9	9	9	3	3			3	1	5	3
Autonomous sensor operation	9				3		1	3		9	1	5	3
Easy to start/control	7				3			1	1	9	1	5	3
Lightweight	6	3	1	1		9	3	3	3			4	5
Durable/reliable	8		3	3		1	3	3	1	3		4	3
Low cost	7	1				3	1	1	9			5	5
Safe to operate	6				9		1	1		9	3	5	5
Fast crossing	5		1		3		9	3			9	2	4
Simple manufacturing/assembly	7	1	3	3		3	1		9	1		5	3
Measurement Unit		cm³	mm	cm²	m/s²	g	W	mAh	¥	ms	cm/s		
Target Value		30000	500	500	1.2	1000	30	2000	1000	100	40		
Total		113	254	249	228	140	233	114	168	286	98		
Normalized		0.06	0.13	0.13	0.12	0.07	0.12	0.06	0.09	0.15	0.05		

Figure 2: Quality Function Deployment matrix for Murphy's Tank.

B Concept Generation

Three existing mobility approaches were considered during concept generation.

Table 2: Mobility approaches considered during concept generation.

Approach	Main advantage	Limitation
Continuous tracks	Provide a long contact region and good traction	Require reliable alignment and tension
Multi-wheel chassis	Simple construction and good load distribution	Individual wheels can lose contact at the gap
Deployable bridge	Creates direct support across the gap	Requires extra mechanisms and a multi-stage motion

Four vehicle concepts were produced by the team:

1. **Suction-assisted transfer rail:** an extendable rail would reach the second table and pull the vehicle across using a suction attachment.
2. **Long multi-wheel chassis:** a long frame with several wheels would keep the mass near the centre and attempt to bridge the gap using vehicle length.
3. **Rack-and-rail bridge:** motor-driven rails would extend from beneath the vehicle to form a temporary bridge.
4. **Tracked vehicle:** front, middle, and rear wheels would be enclosed by continuous treads to provide a larger support region.

C Concept Selection

The four concepts were compared in terms of stability, payload capacity, manufacturing difficulty, mass, and crossing reliability.

Table 3: Comparison of the generated concepts.

Concept	Advantages	Limitations
Suction rail	Positive attachment to the far table	Complex sealing and extension sequence
Multi-wheel chassis	Simple and suitable for a heavy frame	Discrete wheels can still create a tipping point
Rack-and-rail bridge	Provides direct support across the gap	Requires long sliding components and accurate alignment
Tracked vehicle	Maintains a larger support region and uses one continuous motion	Adds mass and requires correct tread tension

The tracked concept was selected in principle because it offered the best combination of load capacity and support continuity. During the first embodiment build, however, the treads were temporarily omitted to minimise mass and manufacturing complexity. The team expected the long six-wheel chassis to cross the gap without the additional tread mass. Testing showed that the wheel-only prototype tipped when the front wheels entered the gap, confirming that chassis length alone did not maintain a support reaction ahead of the centre of mass. The selected tracked concept was therefore completed by connecting the three wheel stations with continuous treads so that support could be maintained on both tables during the crossing.

D Embodiment Design

The selected concept was developed into a six-wheel tracked vehicle with a modular PLA frame, steel reinforcement, two powered shafts, timing-belt transmissions, and an Arduino-based control system. The design was divided into printable frame sections because the complete chassis was larger than the available 3D-printer build volume.

1 Functional Mechanisms

The vehicle required five main functions:

- **Carry the load:** the central frame supports the battery and payload. The PLA structure and steel reinforcement transfer the load to the side frames and shaft supports.
- **Generate propulsion:** two DC gearmotors provide the torque needed to move the vehicle. One motor drives the front shaft and the other drives the rear shaft.
- **Transmit torque:** toothed timing belts transfer motor torque to the wheel shafts. The pulley ratio increases output torque while reducing shaft speed.
- **Maintain support:** three wheel stations guide the treads on each side. The treads allow contact to remain on the near and far tables during the crossing.
- **Control the vehicle:** an Arduino-based system operates the motor drivers and controls the duration and direction of vehicle movement.

2 Structure of Components

The planned design placed the main battery compartment at the centre of the vehicle. The battery was intended to sit directly inside this compartment, with holes added later to allow the wiring to pass through the frame. Openings were positioned immediately in front of and behind the battery compartment for the two motor drivers. The two motors connected to these drivers were to be mounted below them using braces and linked to the front and rear wheel shafts through worm-gear arrangements.

No fixed positions were assigned to the Arduino, its secondary battery, or the breadboard because their masses and dimensions were considered small compared with the main battery, motors, and frame. Their locations could therefore be selected later without significantly changing the centre of mass. The breadboard connected the control wiring and supported the push buttons used to select the vehicle speed and begin the programmed run. A third shaft was positioned below the central battery compartment. This shaft supported the unpowered middle wheels, which were intended to help support the vehicle during the gap crossing.

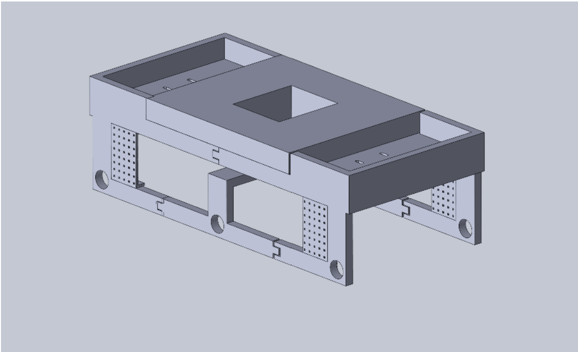

(a) Complete planned frame assembly showing the interlocking frame joints, circular shaft holes, and perforated brace mounting faces that locate and fasten the main modules.

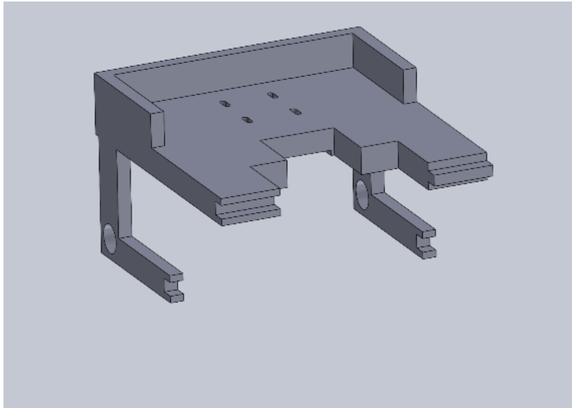

(b) Front or rear frame module showing the slotted connection tabs, motor mounting holes, and shaft opening used to attach it to the central structure.

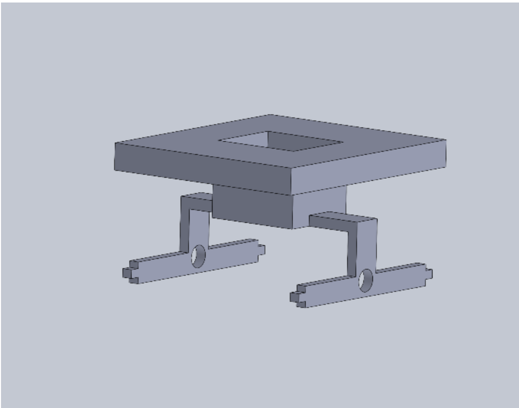

(c) Central frame module showing the battery opening, lower middle-shaft supports, and interlocking rail ends used to join the surrounding sections.

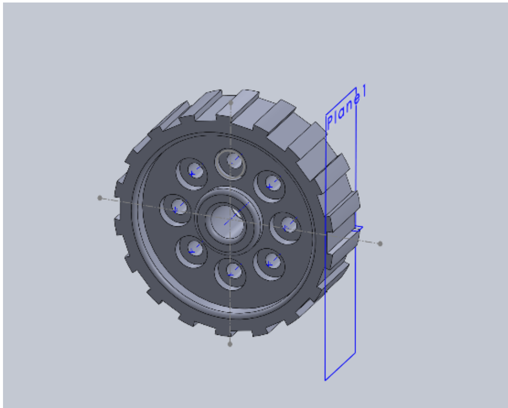

(d) Printed wheel design showing the central shaft bore and outer tread features used to fit the wheel to the axle and engage the track.

Figure 3: CAD models of the planned vehicle components and the locating, fastening, and shaft-support features that make assembly possible.

Two additional methods of carrying removable payload were considered but were not implemented. The first idea was to make a mould and cast concrete weights. Concrete was attractive because it is inexpensive, dense, and can be formed into a required shape. However, this approach was rejected because of the time and uncertainty involved in making a suitable mould and casting the weights ourselves.

The second idea was to print small hollow blocks in two parts, similar to LEGO bricks. The blocks could be filled with sand and sealed, while matching studs on the top of the vehicle would allow several blocks to be attached securely. Sand would have added useful mass at almost no cost, and the printed shells would also have been inexpensive. However, this approach depended on completing the working prototype much earlier so that the payload system could be designed, printed, and tested. It was therefore not implemented.

The final vehicle retained most of the planned frame arrangement but included two major changes. First, the worm-gear transmission was replaced with a belt drive. The motors were repositioned sideways, and toothed belts connected pulleys on the motor outputs to pulleys on the front and rear shafts. Second, the middle wheel assembly was fixed in place and retained mainly as a support point. Continuous treads were then fitted around the front, middle, and rear wheels to maintain contact and improve support during the gap crossing.

3 Material Selection

PLA was selected for the three main frame modules and the six wheels because the parts contained integrated battery compartments, motor pockets, bearing locations, interlocking joints, and other features that could be produced directly by fused-filament fabrication. The material and printing service were readily available, the parts could be revised without machining new tooling, and the low infill fraction limited the structural mass. Published work also shows that the mechanical response of printed PLA depends on infill and print orientation, so the printed geometry and local reinforcement were considered together rather than treating PLA as an isotropic bulk material [2, 3].

Sheet steel was selected for the six local reinforcement plates because the axle openings and leg-to-body transitions reduced the remaining PLA section and created likely stress-concentration regions. Bending each plate into a channel increased its section stiffness, while the continuous steel path carried part of the local tensile and bending load across the printed joints. The combined material strategy therefore used PLA for the large, lightweight and geometrically complex frame modules, while steel was reserved for small regions where local stiffness and damage resistance were more important than mass.

To assess this selection, a static finite element analysis was performed in SolidWorks. The minimum payload objective was 40 kg, while 100 kg was the maximum load the team hoped the frame could support. The 100 kg stretch-load case was represented by an approximately 1000 N downward force on the upper platform, with the lower frame supports fixed and the assembly contacts treated as bonded:

$$W = mg = (100\,\mathrm{kg})\left(9.81\,\mathrm{m/s^2}\right) = 981\,\mathrm{N} \approx 1000\,\mathrm{N}. \tag{1}$$

The maximum resultant displacements of the original and reinforced models were 0.095 54 mm and 0.097 67 mm, respectively. Using the larger value as the conservative result gives

$$k_{\mathrm{eff}} = \frac{F}{\delta_{\mathrm{max}}} = \frac{1000\,\mathrm{N}}{0.097\,67\,\mathrm{mm}} \approx 1.02 \times 10^4\,\mathrm{N/mm}. \tag{2}$$

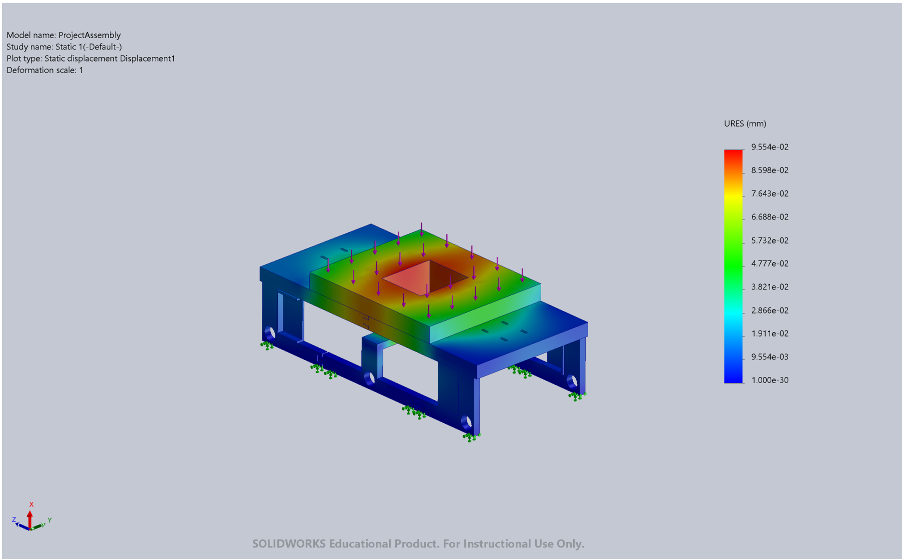

Figure 4: Resultant displacement of the original PLA frame under the approximately 1000 N vertical load.

The reinforced model showed a displacement increase of only

$$\frac{0.09767 - 0.09554}{0.09554} \times 100\% \approx 2.23\,\%, \tag{3}$$

while the reported maximum von Mises stress changed from approximately 47.84 MPa to 49.89 MPa, an increase of about

$$\frac{49.89 - 47.84}{47.84} \times 100\% \approx 4.29\,\%. \tag{4}$$

These small increases do not mean that the steel plates made the physical frame less useful. The two configurations were solved as separate assemblies and therefore used different meshes after remeshing. The reinforced model also introduced additional bonded contacts, local stiffness changes, and extra steel mass. Peak displacement and peak stress are sensitive to mesh density, contact discretisation, and the exact element in which the maximum occurs; where self-weight is included, the added reinforcement mass also contributes a small additional load. The numerical differences are therefore small relative to the modelling changes. The purpose of the plates was mainly to improve the local load path around the circular holes and leg transitions, not necessarily to reduce the single global maximum reported by two separately meshed models.

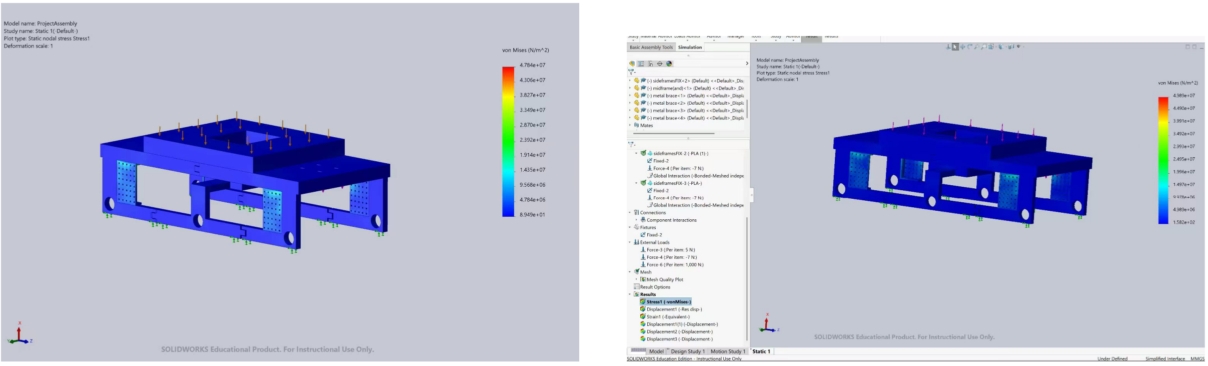

(a) Von Mises stress distribution for the original PLA frame.

(b) Von Mises stress distribution after adding the sheet-steel plates.

Figure 5: Stress distributions from the separately meshed original and reinforced frame models under the approximately 1000 N load.

The reinforced model produced a maximum equivalent strain of

$$\varepsilon_{\max} = 4.042 \times 10^{-4} = 0.04042\%. \tag{5}$$

For a nominal factor-of-safety check, the lower horizontal printed-PLA yield strength of 51 MPa reported in a manufacturer technical data sheet was used as a reference value [11]. Comparing this value with the larger simulated von Mises stress gives

$$\mathrm{FoS}_{\mathrm{nom}} = \frac{\sigma_{\mathrm{ref}}}{\sigma_{\mathrm{vM,max}}} = \frac{51\,\mathrm{MPa}}{49.89\,\mathrm{MPa}} \approx 1.02. \tag{6}$$

This nominal value is only slightly above unity, so the steel plates were retained to reduce reliance on the narrow PLA sections around the axle holes and frame-leg connections. The physical 75 kg flat-floor load test provided an additional practical check: the vehicle moved without visible fracture or permanent bending. Together, the FEA and the test supported the use of a lightweight printed PLA frame with local sheet-steel reinforcement.

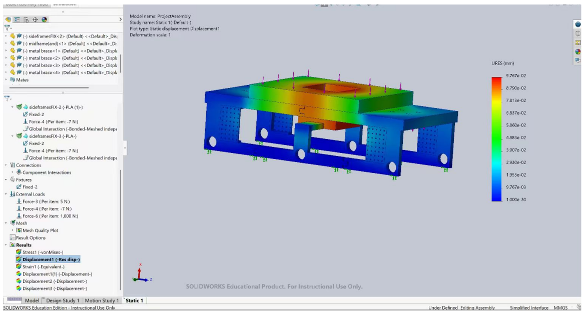

(a) Resultant displacement of the reinforced frame.

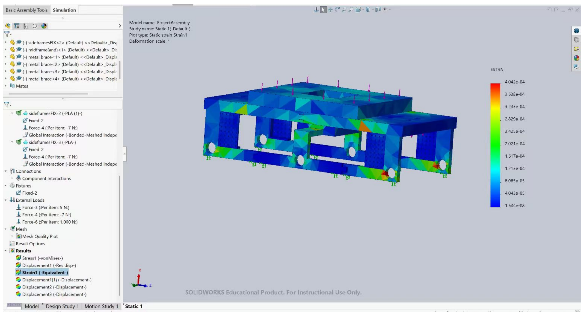

(b) Equivalent strain distribution of the reinforced frame.

Figure 6: Displacement and equivalent strain results for the sheet-steel-reinforced frame.

4 Engineering Analysis

Quasi-Static Stability Analysis and the Tipping Problem. Our initial design merely consisted of six wheels with the front and rear wheels driving the car forward. We realized that this design consistently led to tipping as soon as the car encountered the gap. To understand this, we perform a simple static analysis. Under this assumption, the vehicle must remain in static equilibrium at every position during the crossing. Therefore, the vertical projection of the centre of mass must remain within the region bounded by the wheel contact points supporting the vehicle.

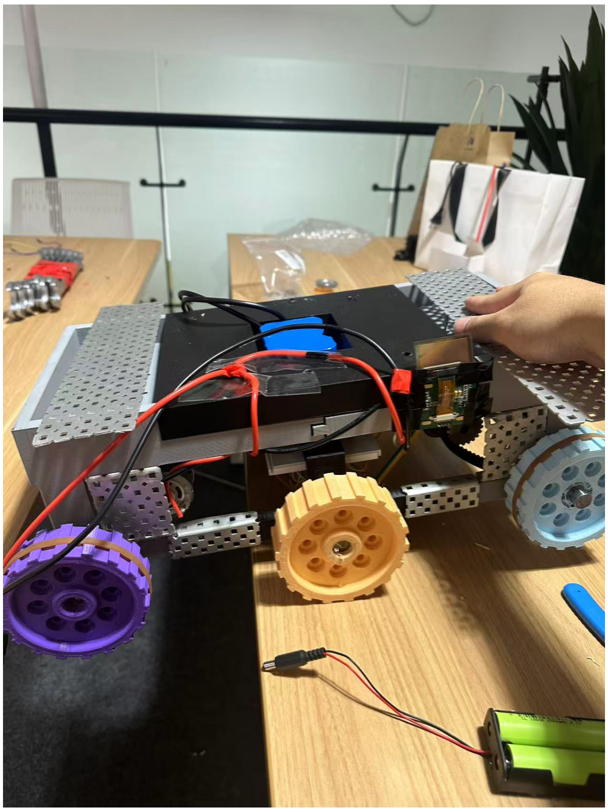

Figure 7: Our initial design shown tipping.

Because the vehicle is symmetric about its longitudinal centreline, the left and right wheels at each position can be treated as a single equivalent axle in the side-view analysis. The vehicle can therefore be represented using three equivalent wheel contact points: the front, middle, and rear wheel pairs. The centre of mass is assumed to be located at the geometric centre of the vehicle, approximately above the middle wheel pair.

Let s denote the centre-to-centre distance between two consecutive wheel pairs, and let G denote the width of the gap. For the initial design, the measured wheel spacing and gap width were

$$s = 18.5\,\text{cm} = 0.185\,\text{m}, \tag{7}$$

$$G = 20\,\text{cm} = 0.200\,\text{m}. \tag{8}$$

Therefore, the wheel spacing was smaller than the width of the gap:

$$s < G. \tag{9}$$

The difference between the gap width and the wheel spacing was

$$\Delta = G - s. \tag{10}$$

Substituting the measured dimensions gives

$$\begin{aligned}
\Delta &= 0.200\,\mathrm{m} - 0.185\,\mathrm{m} && (11)\\
&= 0.015\,\mathrm{m} && (12)\\
&= 1.5\,\mathrm{cm}. && (13)
\end{aligned}$$

This result means that when the middle wheel reached the near edge of the gap, the front wheel was still approximately 1.5 cm short of the far platform. The front wheel could not establish contact with the far platform before losing contact with the near platform. The vehicle therefore had to pass through a configuration in which the front wheels were unsupported.

Let N_F, N_M, and N_R represent the vertical normal reactions acting at the front, middle, and rear wheel pairs, respectively. Let m be the total mass of the vehicle and g be gravitational acceleration. Vertical force equilibrium requires

$$\sum F_y = 0. \tag{14}$$

Therefore,

$$N_F + N_M + N_R - mg = 0, \tag{15}$$

or equivalently,

$$N_F + N_M + N_R = mg. \tag{16}$$

As the front wheels passed beyond the edge of the near platform, they lost contact with the supporting surface. The front-wheel normal reaction therefore became zero:

$$N_F = 0. \tag{17}$$

The vertical force-equilibrium equation then reduced to

$$N_M + N_R = mg. \tag{18}$$

At this stage, the middle-wheel contact became the critical point for evaluating the stability of the vehicle. Let e represent the horizontal distance between the vertical projection of the centre of mass and the middle-wheel contact point. A positive value of e indicates that the centre of mass is located ahead of the middle wheel in the direction of travel.

Taking moments about the middle-wheel contact eliminates the middle-wheel reaction N_M, because its line of action passes directly through the selected moment point. Taking the forward tipping direction as negative, the moment-equilibrium equation is

$$\sum M_M = N_F s - N_R s - mge = 0. \tag{19}$$

Immediately after the front wheels lost contact with the platform, $N_F = 0$. The moment-equilibrium equation therefore became

$$-N_R s - mge = 0. \tag{20}$$

Solving for the rear-wheel reaction gives

$$N_R = -\frac{mge}{s}. \tag{21}$$

Under the ideal assumption that the centre of mass is located directly above the middle-wheel contact point,

$$e = 0. \tag{22}$$

Substituting this condition into the expression for the rear-wheel reaction gives

$$N_R = 0. \tag{23}$$

The vertical force-equilibrium equation consequently becomes

$$N_M = mg. \tag{24}$$

This result indicates that, at the instant the front wheels lost contact, the entire weight of the vehicle was theoretically supported by the middle wheel pair. At the same time, the rear wheel pair became unloaded. The middle-wheel contact was therefore the only effective support point and became the pivot about which the vehicle could rotate.

This configuration represents marginal equilibrium rather than stable equilibrium. The projection of the centre of mass lies at the forward boundary of the remaining support region instead of lying securely inside it. The vehicle could theoretically remain balanced only if the centre of mass were positioned exactly above the middle-wheel contact and if no disturbances, dimensional variations, or forward displacement occurred.

In the physical prototype, exact alignment between the centre of mass and the middle-wheel contact could not be maintained. Factors such as battery placement, motor placement, wiring, chassis flexibility, unequal component masses, wheel tolerances, and continued forward movement could shift the effective centre of mass slightly ahead of the middle wheel. In this case,

$$e > 0. \tag{25}$$

The corresponding rear-wheel reaction would then be

$$N_R = -\frac{mge}{s} < 0. \tag{26}$$

A negative normal reaction is physically impossible because the ground can exert an upward force on the rear wheels but cannot pull the wheels downward. Therefore, no physically possible combination of wheel reactions can maintain static equilibrium once the centre of mass moves ahead of the middle-wheel contact.

The weight of the vehicle then produces an unbalanced forward moment about the middle wheel. The magnitude of this tipping moment is

$$M_{\text{tip}} = mge. \tag{27}$$

Since the front wheels are unsupported and the rear wheels are unloaded, there is no opposing moment available to balance this gravitational moment. The middle-wheel contact consequently acts as the pivot point, and the vehicle begins rotating forward into the gap.

The quasi-static analysis therefore explains the tipping observed during testing. The failure occurred immediately after the front wheels lost contact with the near platform. At this instant, the support condition reduced from three wheel pairs to the middle and rear wheel pairs. However, because the centre of mass was positioned at or slightly ahead of the middle-wheel contact, the rear wheels could not provide a stabilising reaction. The middle wheel became the moment-imbalance point and the effective pivot of the vehicle. Even a small forward displacement of the centre of mass produced an unbalanced gravitational moment, causing the vehicle to tip forward.

To eliminate this single-point tipping condition, continuous tracks were fitted around the three wheels on each side of the vehicle. During the critical stage of the crossing, the tracks remained in contact with both the near and far platforms, as shown in Figure 8. The distributed contact pressures on the two platforms can be replaced by equivalent vertical reactions N_{near} and N_{far}, acting at their respective centres of pressure x_{near} and x_{far}. If x_C is the horizontal position of the centre of mass, static stability requires $x_{\text{near}} < x_C < x_{\text{far}}$. The force and moment equilibrium equations for the tracked vehicle are therefore

$$N_{\text{near}} + N_{\text{far}} = mg, \tag{28}$$

$$N_{\text{far}}(x_{\text{far}} - x_C) - N_{\text{near}}(x_C - x_{\text{near}}) = 0. \tag{29}$$

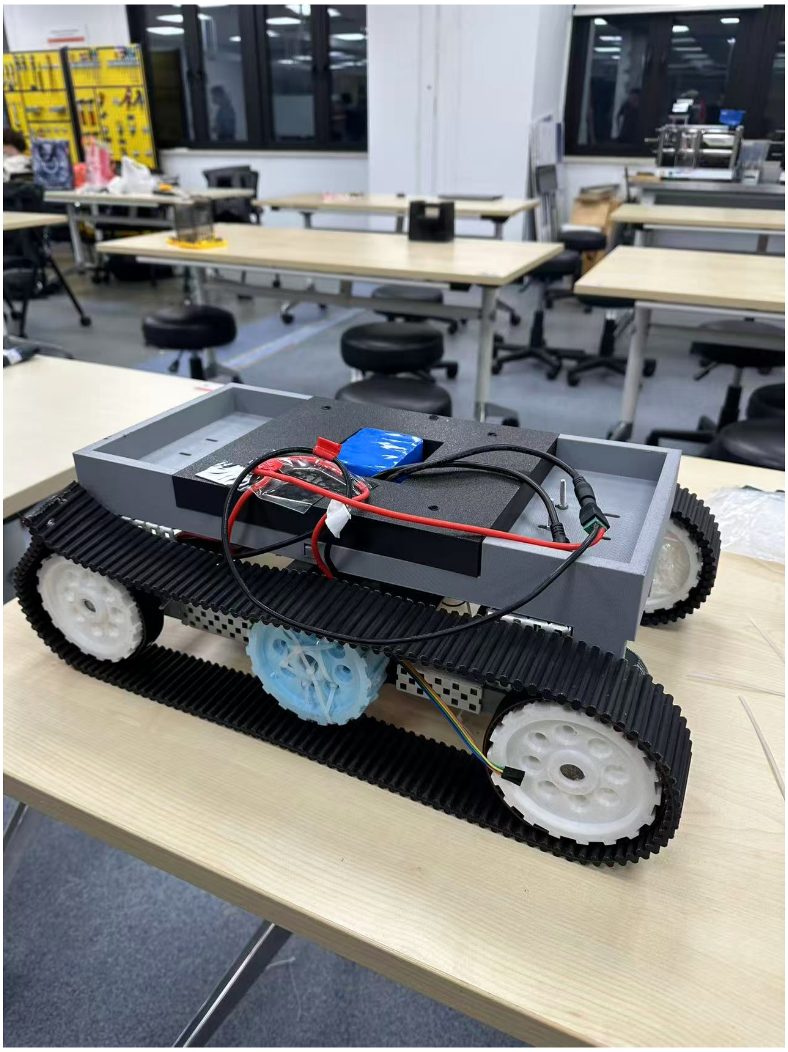

Figure 8: The modified tracked design used in the one successful official gap-crossing trial.

Solving the two equilibrium equations gives

$$N_{\text{near}} = mg\frac{x_{\text{far}} - x_C}{x_{\text{far}} - x_{\text{near}}}, \tag{30}$$

$$N_{\text{far}} = mg\frac{x_C - x_{\text{near}}}{x_{\text{far}} - x_{\text{near}}}. \tag{31}$$

Because the centre of mass lies between the two effective track reactions, the distances $x_{\text{far}} - x_C$, $x_C - x_{\text{near}}$, and $x_{\text{far}} - x_{\text{near}}$ are all positive. Consequently,

$$N_{\text{near}} > 0 \qquad \text{and} \qquad N_{\text{far}} > 0. \tag{32}$$

Both platforms therefore provide physically possible upward reactions throughout the critical portion of the crossing. These reactions produce moments in opposite directions about the centre of mass, and static equilibrium is maintained because

$$N_{\text{near}}(x_C - x_{\text{near}}) = N_{\text{far}}(x_{\text{far}} - x_C). \tag{33}$$

This is fundamentally different from the original wheel design. When the front wheel lost contact in the original design, $N_F = 0$, and the moment equation about the middle wheel required

$$N_R = -\frac{mge}{s}. \tag{34}$$

For $e > 0$, this would require a negative rear-wheel reaction, which is impossible. The rear wheel therefore became unloaded, leaving the middle wheel as the pivot. With tracks, two separated support reactions remained on opposite sides of the centre of mass, allowing the moment produced by the vehicle weight to be continuously balanced. When the centre of mass was midway between the two effective track reactions,

$$x_C = \frac{x_{\text{near}} + x_{\text{far}}}{2}, \tag{35}$$

the load was shared equally:

$$N_{\text{near}} = N_{\text{far}} = \frac{mg}{2}. \tag{36}$$

The main benefit of the tracks was therefore not simply an increase in contact area. The tracks maintained an extended support region across the gap and kept the centre of mass between two positive vertical reactions. This removed the single-point middle-wheel pivot present in the original design and allowed the vehicle load to transfer progressively from the near platform to the far platform without producing an unavoidable tipping moment. This explains why, during the successful official trial, the front wheels were able to traverse the 20 cm clear gap without the middle-wheel tipping failure observed in the original design.

5 Control Mechanism

The goal of the control system is to let an operator select a drive speed, start a crossing, and have the vehicle traverse the obstacle and stop by itself after a fixed run time, without any tether or remote link. All command input and all feedback therefore happen on the vehicle itself. As in the mechanical design, the message flow is split into three parts: the *controller*, the *driver*, and the *actuator*. Fig. 9 shows the logic of the system together with the voltage domain of each connection.

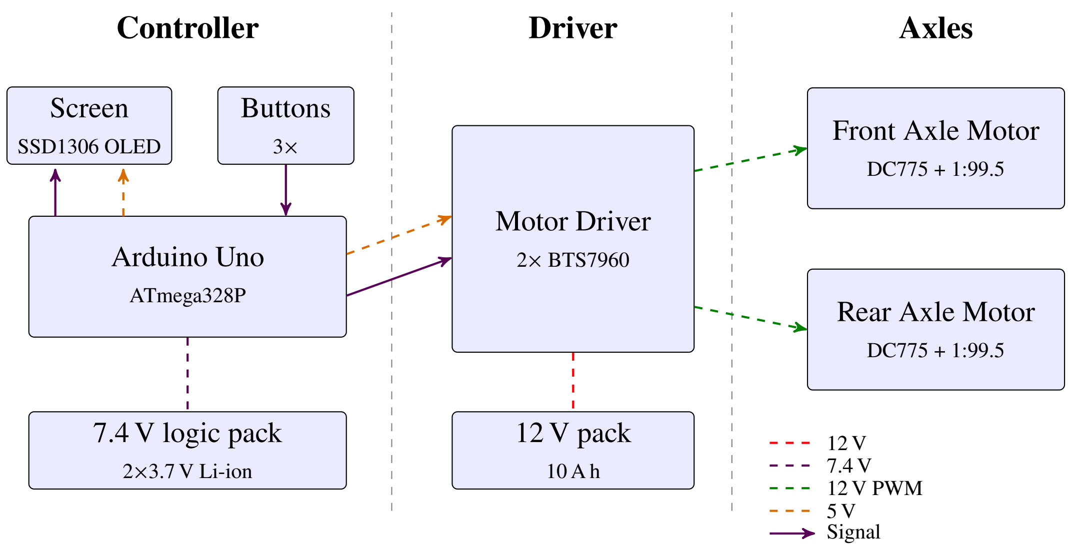

Figure 9: Overall system block diagram, showing the three voltage domains and the direction of signal flow.

Controller. The controller is an Arduino Uno built around the ATmega328P [5, 6], powered from a 7.4 V pack of two 3.7 V lithium-ion cells in series feeding the barrel jack. It is the only element of the system that holds state. Operator input is read from three momentary tactile switches wired to digital pins D2, D3 and D4 and configured as `INPUT_PULLUP`, so no external pull-up resistors are required and a pressed button reads `LOW`. Feedback is presented on a 128×64 SSD1306 OLED module on the I^2C bus (A4/A5), driven by the U8g2 library in page-buffer mode [7, 9]. Page buffering was chosen deliberately: a full 128×64 frame buffer would occupy 1024 bytes, half of the 2 kB of SRAM on the ATmega328P, whereas the page buffer renders the frame in eight strips and costs an eighth of that [6, 7]. The complete pin allocation is given in Table 4.

Table 4: Controller pin allocation.

Pin	Signal	Direction	Function
D2	`BTN_UP`	In (pull-up)	Increase set speed by 5 %
D3	`BTN_DOWN`	In (pull-up)	Decrease set speed by 5 %
D4	`BTN_START`	In (pull-up)	Latch run state, begin crossing
D5	`L_RPWM`	Out (PWM)	Channel L forward, Timer0, 977 Hz
D6	`L_LPWM`	Out (PWM)	Channel L reverse, Timer0, 977 Hz
D7	`L_EN`	Out	Channel L half-bridge enable
D8	`R_EN`	Out	Channel R half-bridge enable
D9	`R_RPWM`	Out (PWM)	Channel R forward, Timer1, 490 Hz
D10	`R_LPWM`	Out (PWM)	Channel R reverse, Timer1, 490 Hz
A4/A5	`SDA/SCL`	Bidirectional	OLED display bus

Driver. Each motor is fed by its own BTS7960 (IBT-2) module, a pair of half-bridges built from one high-side and one low-side MOSFET each. The module accepts two PWM inputs, `RPWM` and `LPWM`, and an enable line per bridge; commanding one input and holding the other at zero sets the direction, so direction and magnitude are carried on the same two wires. In firmware the two modules are designated channel L and channel R, which map to the front-axle and rear-axle drivers respectively. The BTS7960 datasheet specifies a typical current-limitation level of 43 A rather than a guaranteed continuous module current rating [8]. The selected motor data gave a nominal current of $38.4\,\mathrm{W}/12\,\mathrm{V} = 3.2\,\mathrm{A}$ per motor, which is below this protection threshold. The actual continuous current capability still depends on the module cooling, PCB construction and ambient conditions. The available current margin is useful during start-up and near-stall operation, when motor current can rise above its nominal running value. The logic side of each module is powered from the Arduino 5 V rail and the power side from the 12 V pack, with the two grounds tied together at a single point so that the PWM signals have a defined reference.

Actuator and drivetrain coupling. The vehicle carries six wheels on three axles and two DC775 motors, each fitted with a 1:99.5 planetary gearbox giving 60 rpm at no load and 32 kgf·cm of rated torque. One motor is mounted to the front axle and one to the rear. The centre wheel pair was initially undriven and free to rotate, but after the tipping tests it was rigidly attached to the frame and the two centre-shaft journal bearings were removed. Torque is transmitted from each gearbox output to its axle through a toothed pulley and belt with a 2:1 reduction, which halves the shaft speed and doubles the torque. In SI units the rated gearbox torque is

$$T_{\mathrm{motor}} = 32\,\mathrm{kgf} \cdot \mathrm{cm} \times 0.0980665 = 3.14\ \mathrm{N} \cdot \mathrm{m}, \tag{37}$$

so each axle receives $2 \times 3.14 = 6.28\ \mathrm{N} \cdot \mathrm{m}$ and the two driven axles together deliver $12.55\ \mathrm{N} \cdot \mathrm{m}$ at the wheels. Using the nominal gearbox data, the assumed 2:1 reduction leaves the axles turning at 30 rpm. With 50 mm wheels, the corresponding pre-test kinematic estimate is

$$v_{\mathrm{nom}} = \frac{n_{\mathrm{axle}}}{60}\pi d = \frac{30}{60} \times \pi \times 0.05 = 0.0785\ \mathrm{m/s}. \tag{38}$$

The 200 mm challenge dimension is the clear gap traversed by the front wheels; it is not the complete timed travel distance. The official stopwatch was stopped only after the whole 520 mm-long vehicle cleared the end line. Taking the minimum case in which the vehicle front begins at the start line, the front of the vehicle travels at least

$$L_{\mathrm{run}} = 0.20\,\mathrm{m} + 0.20\,\mathrm{m} + 0.20\,\mathrm{m} + 0.52\,\mathrm{m} = 1.12\,\mathrm{m}, \tag{39}$$

where the terms represent the start-line offset, gap width, end-line offset, and vehicle length. The successful 6 s run therefore corresponds to a minimum average course speed of

$$v_{\text{course}} = \frac{L_{\text{run}}}{t} = \frac{1.12\,\text{m}}{6\,\text{s}} \approx 0.187\,\text{m/s}. \tag{40}$$

Because the vehicle began behind the start line, its true travel distance and average speed were slightly larger. The difference between the observed course speed and the nominal kinematic estimate shows that the nominal motor speed, effective belt ratio, or effective tread diameter did not fully represent the assembled prototype. The measured course result is therefore used when reporting the tested performance.

Table 5: Drivetrain parameters at full PWM command.

Parameter	Value	Source
Motor	2× DC775, 12 V	Selected
Gearbox ratio	1:99.5	Datasheet
Gearbox output speed	60 rpm (no load)	Datasheet
Gearbox rated torque	32 kgf·cm = 3.14 N · m	Datasheet
Rated power	38.4 W per motor	Datasheet
Belt reduction	2:1	Design
Torque per driven axle	6.28 N · m	Eq. (37)
Total tractive torque	12.55 N · m	Eq. (37)
Axle speed	30 rpm	Design
Wheel diameter	50 mm	Design
Nominal speed estimate	0.0785 m/s	Eq. (38)
Minimum measured course speed	0.187 m/s	Eq. (40)

Power architecture. Power is deliberately split across two separate packs rather than taken from a single source, as shown in Fig. 10. The 12 V, 10 A h pack supplies only the motor rails of the two BTS7960 modules; the 7.4 V pack supplies the Arduino, and through the Arduino regulator the display, the buttons and the logic side of both drivers. The reason is brownout. A brushed DC motor drawing its stall current collapses the bus voltage for several milliseconds, and if the microcontroller shared that bus the resulting dip below the regulator dropout would reset the ATmega mid-crossing with the drivers still enabled. Splitting the packs means the worst the motor transient can do is disturb the shared ground reference. At the rated draw of 6.4 A for both motors, the motor pack stores

$$E = 12\,\text{V} \times 10\,\text{A h} = 120\,\text{W h}, \qquad t = \frac{120}{2 \times 38.4} \approx 1.6\,\text{h} \tag{41}$$

of continuous running, which against an 8 s crossing is far more than the mission requires; the pack was sized for current delivery during stall rather than for endurance.

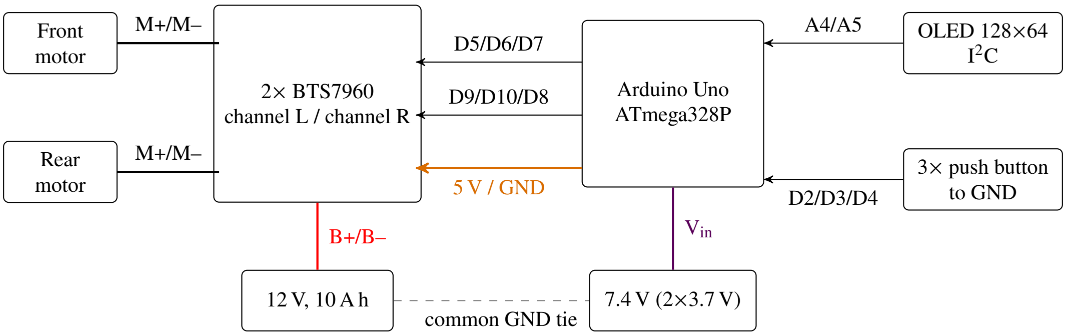

Figure 10: Circuit interconnection diagram. Heavy lines carry motor current; the two packs share a common ground tie so that the PWM signals have a defined reference.

Control logic. The firmware is a two-state machine, shown in Fig. 11. In the IDLE state the motors are held off and the up and down buttons adjust a set-point `speedPercent` between 0 and 100 % in steps of 5 %. Pressing START with a non-zero set-point latches `running`, records the current `millis()` value as `runStart`, and issues the drive command. In the RUNNING state the loop compares elapsed time against `RUN_MS` and calls `motorsOff()` once the crossing window expires, returning the machine to IDLE. With `RUN_MS` set to 8 s, the operator trims the travel distance by adjusting the PWM set-point rather than the programmed time. The nominal drivetrain estimate predicted 0.0785 m/s, whereas the successful official run gave a minimum measured average of 0.187 m/s over the complete course. This difference confirms that the timed controller must be calibrated from physical trials rather than from nominal motor speed alone.

Each button is handled by a small debounce structure that stores the last raw level, the last stable level and the time of the most recent change; a press is only reported when the raw level has been stable for longer than `DEBOUNCE` = 30 ms and differs from the stable level. This edge detection matters here because a single bounce on START would otherwise be read as a start followed immediately by a second start, resetting the timer mid-crossing.

The set-point is converted to a duty cycle by `percentToPwm()`, a linear map from 0–100 % onto the 0–255 range of `analogWrite()`, clamped by `constrain()` [10]. A minimum-duty floor `MIN_PWM` is provided in the mapping so that the map can be rebased onto the

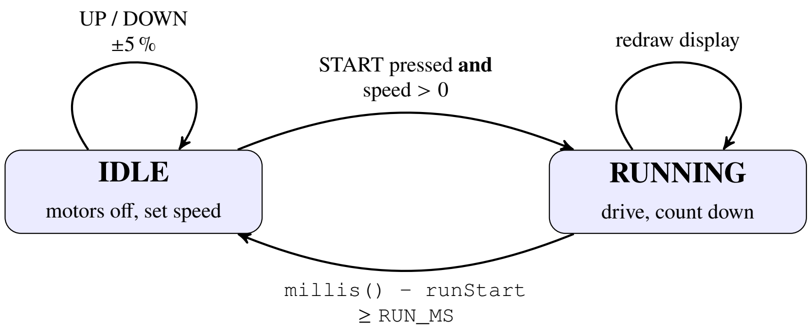

Figure 11: Firmware state machine. Speed can only be changed while idle, so the command is fixed for the duration of a crossing.

smallest duty that actually breaks static friction; it is currently set to zero and the map is a plain proportional one. `driveForward()` then writes the duty to `L_RPWM` and `R_RPWM` while holding `L_LPWM` and `R_LPWM` at zero, and both enable lines are held high for the whole mission. Stopping is done by `motorsOff()`, which zeroes all four PWM outputs with the enables still high; this leaves both low-side devices conducting, so the motors are electrically braked rather than left to coast, and the vehicle stops within a wheel revolution.

Operator display. The display is redrawn once per loop iteration and shows one of two screens. While idle it reads SELECT SPEED above the set-point in large type, with a horizontal bar whose fill is mapped from the percentage. While running it reads RUNNING, the commanded speed, and the remaining time to a tenth of a second, with the bar mapped from the remaining milliseconds so that it empties as the crossing proceeds. One further protection is applied at start-up: `Wire.setWireTimeout(5000, true)` arms a 5 ms timeout with automatic bus reset on the I^2C peripheral [9]. Without it, a display that glitches the bus low would block the `Wire` library indefinitely and hang the main loop — and because the motors are commanded outside the display code, a hang after the drive command would leave the vehicle running with no way to reach the stop check. The core firmware used to implement the timed control sequence is provided in Appendix D. The listing includes the conversion of the selected speed percentage into a PWM duty cycle, the transition between the idle and running states, and the automatic motor shut-off after the programmed run time.

Limitations of the present scheme. The control loop is open-loop, so the selected percentage sets a PWM duty cycle rather than a measured vehicle speed. The actual speed changes as the battery discharges and as the drivetrain load varies, and the nominal motor and transmission data did not reproduce the average speed observed in the successful official trial. The operator therefore adjusted the set-point between runs using physical testing. The two channels drive the front and rear axles rather than the left and right sides, so commanding them differently changes the front-to-rear torque distribution but does not provide steering. A future design would require independent left- and right-side drive if steering were needed.

III Manufacturing

The prototype combines two manufacturing routes. All of the custom structural parts were 3D printed in polylactic acid (PLA), while the rotating, load-carrying and electrical parts were bought as standard components and fitted into features printed directly into the frames. Sheet metal braces were made in the metal shop and added at the end of the build. The finished vehicle measures $520 \times 310 \times 180$ mm and weighs 6.0 kg.

Two constraints shaped these choices: mass and symmetry. Since the crossing manoeuvre depends on where the centre of gravity (CG) sits relative to the unsupported span, added weight and any side-to-side CG offset both hurt performance directly. 3D printing let us build the motor pockets, bearing seats and electronics compartments into the frames themselves, which removed a number of brackets and fasteners along with their tolerance stack-ups. It also meant the heaviest parts were positioned by the printed geometry rather than by how carefully we placed them during assembly.

A Components

1 Structural Frames

The chassis is made up of three printed parts, one mid frame and two mirrored side frames, shown at the left of Fig. 15. All three were printed in PLA through the Shanghai Jiao Tong

University Student Innovation Center machining service platform at its default infill of 15%. We kept this infill setting for all three frame components.

PLA was chosen over machined aluminium or laser-cut acrylic mainly on stiffness-to-weight grounds. The frames are loaded mostly in bending, and a printed section can be made deep, and therefore stiff, at very little weight cost because at 15% infill the interior is largely air. Infill density and pattern can also change the mechanical response of FDM-printed parts [2]. The second reason was feature integration. The motor pockets, bearing bores, battery bay and controller compartments are internal, non-prismatic features that a laser cutter cannot produce at all and that would need several setups to mill. Printing was also cheap to iterate: a revised frame could be resubmitted and reprinted for the cost of the material, which mattered because the internal layout changed several times as the CG analysis developed.

Two things about the print service affected our schedule. Jobs are queued and priced by a points formula based on part volume, scale factor, infill fraction and material colour, so a geometry change costs both points and waiting time. On top of that, one of the two print locations suspended service partway through the project, which pushed all demand onto the remaining facility and made the queue considerably longer. We responded by batching our submissions and sending them as early as the design allowed, and by holding back small design changes until enough had accumulated to justify a single reprint.

The two side frames are mirror images of each other. Each carries three bearing bores for the axles, a recessed motor pocket with its mounting hole pattern, and downward frame members that support the axle and bearing regions and transfer their loads into the upper frame. The mid frame is the spine of the vehicle. It ties the side frames together, fixes the track width, and holds the battery bay along with two symmetric compartments for the motor control electronics.

2 Axles, Bearings and Wheels

Three 15 mm-diameter steel shafts, each 280 mm long, were purchased and used in the vehicle. Six journal bearings were purchased for the original free-running three-axle arrangement. In the final prototype, the front and rear shafts remained rotating axles and used two bearings each.

The middle shaft and wheel pair were rigidly attached to the frame after the tipping tests, so the two middle-shaft bearings were removed. The final assembly therefore used three shafts, four journal bearings, and six wheels.

We used journal bearings instead of ball bearings for reasons of weight and packaging. At the shaft speeds and radial loads involved, a plain sleeve carries the load at lower mass and with a much smaller outside diameter than an equivalent rolling-element bearing, so the bearing bosses and the surrounding frame section could stay thin. A sleeve also copes better with the slight angular misalignment that is unavoidable in a printed frame; a rigidly seated ball bearing would bind and wear under that kind of edge loading.

The bearings were pressed into the printed bores as an interference fit. We preferred this to a clearance fit with adhesive because the press fit locates the bearing concentrically and holds it axially in one operation, and because glued joints on printed parts tend to peel at the layer interface rather than fail in the adhesive. The bore diameters in the CAD model included an allowance for the first-layer expansion and thermal shrinkage typical of FDM parts, so the printed bore gave the interference we wanted without any post-machining.

The wheels were held on the shafts by a deliberate interference fit. We dimensioned the mating features undersize in CAD and forced the wheels onto the shafts. The friction from the interference carries the drive torque and locates the wheels axially at the same time, so no keys, grub screws or collars were needed. The trade-off is that taking a wheel off again tends to damage it.

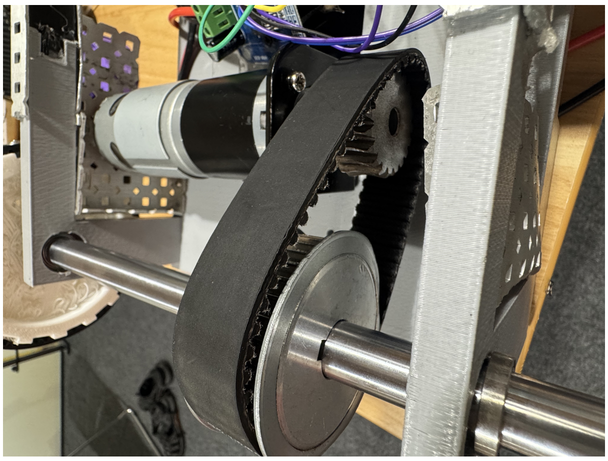

Figure 12: The drivetrain, shaft, and bearing

3 Drive Transmission

Torque reaches the axles from the gearmotors through HTD 300-5M synchronous timing belts running on toothed pulleys. The designation means a 5 mm tooth pitch and a 300 mm pitch length, so each belt has 60 teeth [4]. Belts let us mount the motors away from the axle line, which was necessary to keep these heavy parts inboard for CG reasons. When correctly tensioned, a toothed belt transmits torque without relative tooth slip, so wheel rotation remains predictable for the automated crossing sequence [4]. The belt also has enough compliance to absorb part of the shock when a wheel reaches the far table edge instead of passing it directly into the gearbox.

Figure 13: Drive-transmission system isolated

4 Fasteners and Reinforcement

The frames are joined by roughly 16 machine screws with nuts, plus five or six self-tapping screws. The two types do different jobs. Through-bolted joints with nuts are used at the side-frame-to-mid-frame interfaces, where we needed to open the joint repeatedly and where the clamping load can be reacted on both faces. Self-tapping screws are used where only one side is accessible and the screw has to thread straight into the printed PLA. Their coarse, sharp thread form cuts its own path and develops a large engagement area in a soft, low-strength material, which a machine screw in a plain hole would not do.

Six sheet steel braces were added after the first round of testing. They can be seen at the lower right of Fig. 15 and installed on the vehicle in Fig. 16. Each was cut from flat steel sheet, bent on three sides into a channel section, deburred, and drilled to match the frames. The bending is what makes the brace work. A flat strip has almost no second moment of area about its weak axis, but turning up the edges moves material away from the neutral axis and raises the section stiffness by more than an order of magnitude for the same weight of steel. The perforations remove material from near the neutral axis, where it does least for stiffness, so the weight penalty stays small.

The braces are fastened across the leg-to-body transitions of the side frames, which are the most highly stressed regions in the structure. The legs behave as cantilevers whenever the vehicle overhangs the gap, so the inside corner where a leg meets the main body is both the section of maximum bending moment and a geometric stress raiser. That corner is also a bad place to rely on a printed part, since it lies on the inter-layer bond plane, which is commonly a weak direction in an FDM component because printed properties depend strongly on build and raster orientation [3]. Bridging the corner with continuous steel puts the tensile side of the bending load into the brace rather than into the layer adhesion of the PLA.

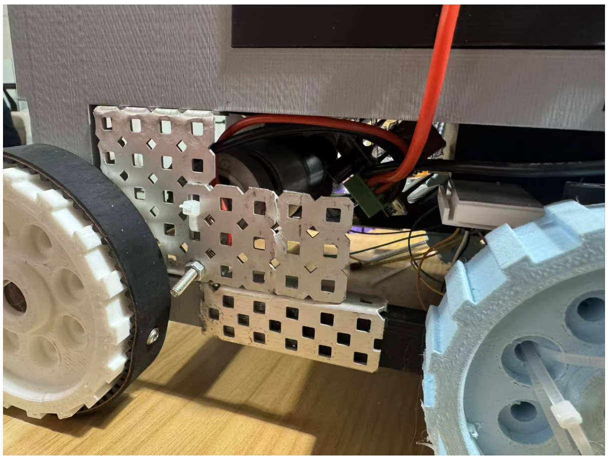

Figure 14: Sheet-metal reinforcement

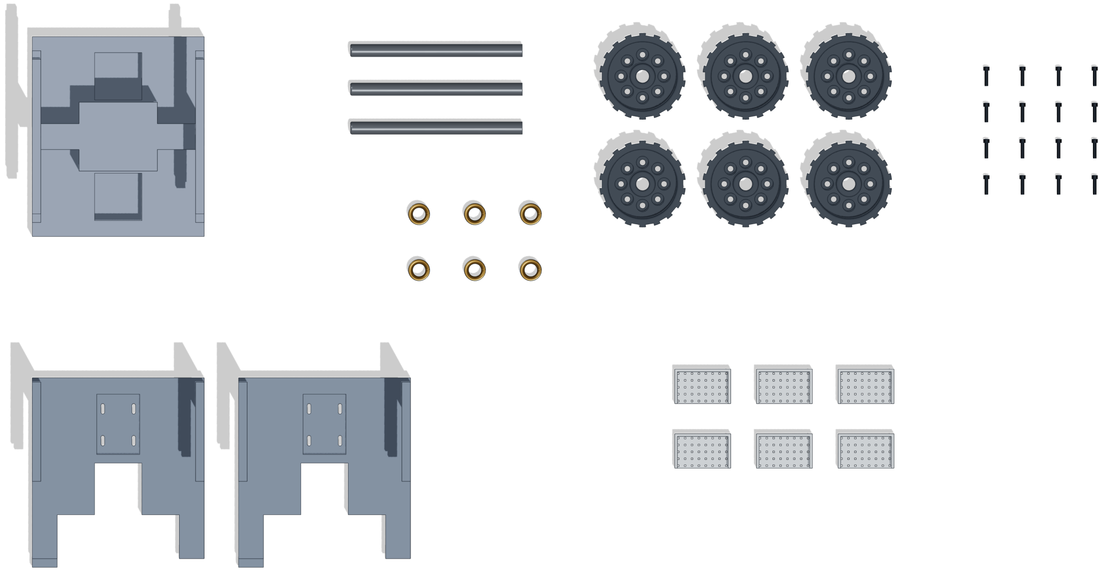

Figure 15: Exploded view of the prototype showing all manufactured and purchased components: mid frame, three shafts, six wheels, the six journal bearings purchased for the original arrangement, fasteners, two mirrored side frames and six sheet steel reinforcing braces.

B Assembly

The assembly order follows from how the parts nest inside one another. Each stage closes off the one before it, so getting a step out of order means taking the whole vehicle apart again to fix it. We used the following sequence for every rebuild.

Step 1: Frame subassembly. The mid frame was bolted between the two side frames. This step sets every datum that follows: track width, axle parallelism, and the symmetry plane of the vehicle. We left all fasteners finger-tight until the three frames were mated, then tightened them in a diagonal pattern so the frames pulled up square instead of skewing about whichever joint was tightened first.

Step 2: Bearing installation. The six journal bearings were initially pressed into their bores, three per side frame, for the free-running three-axle prototype. Each pair was checked with a test shaft to confirm free rotation. After the tipping tests, the two bearings assigned to the middle shaft were removed because the middle shaft and wheel pair were rigidly fixed to the frame. The final vehicle retained four journal bearings, two for the front shaft and two for the rear shaft.

Step 3: Shafts and wheels. The front and rear shafts were passed through their bearing pairs, and the wheels were forced onto the exposed ends. These two rotating axles were turned by hand to check for binding. The middle shaft and wheel pair were then aligned at the centre position and rigidly secured to the frame, where they acted as a fixed support beneath the tread rather than as a free-running axle.

Step 4: Motors and transmission. The geared motors were seated in the pockets in the side frames and screwed down through the printed hole pattern, then the HTD 300-5M belts were fitted over the motor and axle pulleys. Because the pockets are part of the frame, the belt centre distance is set by the printed geometry. This simplified assembly, but it also left no adjustment for print tolerance, belt stretch, or wear, which later contributed to belt looseness and slip.

Step 5: Electronics and power. Most of the electronics sits at the rear of the vehicle. The battery, which is by some margin the heaviest single component, goes in its own compartment at the centre of the mid frame. We designed it this way because the crossing manoeuvre is only stable while the CG stays within a narrow longitudinal band relative to the supported span. Putting the battery at the centre keeps the CG on the vehicle centreline and near mid-span, and the compartment is sized so the pack cannot shift during operation. The two motor control compartments in the mid frame are mirrored about the same centreline, so the control electronics add no net side-to-side moment. Any imbalance left over would show up as yaw drift during the crossing, which is exactly when the vehicle can least afford to correct it.

Step 6: Reinforcement. The six sheet steel braces were screwed across the leg regions of the side frames last, three per side, keeping the symmetry set up in Step 1. They went on at the end because they span joints made in the earlier steps, and leaving them until last avoids having to remove them for any further access to the drivetrain or the electronics.

Fig. 16 shows the finished prototype. Its measured mass is 6.0 kg and its overall envelope is $520 \times 310 \times 180$ mm.

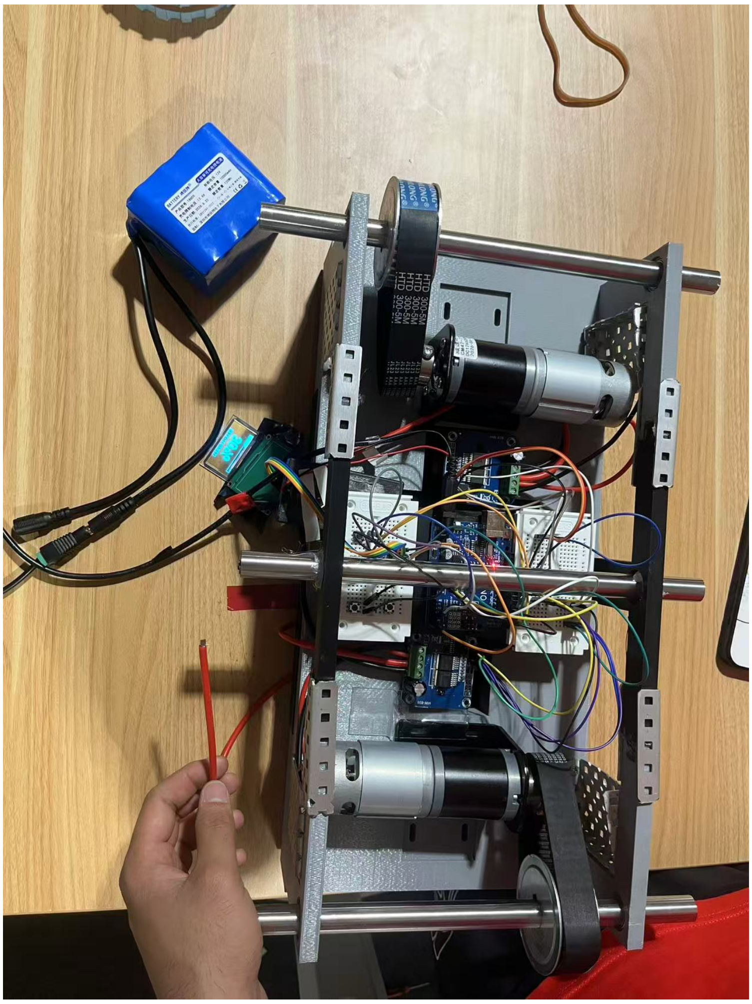

Figure 16: Assembled prototype, plan view, showing the belt-driven axles, the battery pack in its central compartment, the symmetric motor control compartments in the mid frame, and the sheet steel braces across the leg transitions on both side frames.

IV Cost

The project cost was divided into two categories. The final-prototype cost includes purchased parts retained in the completed vehicle, while the overall development cost includes components purchased for earlier concepts, modifications, and planned testing. The out-of-pocket final-prototype cost was RMB 399.60, while the complete development process cost RMB 769.60. The frame modules and six wheels were 3D printed through the university service at no direct RMB purchase cost to the team. The treads, pulleys, fasteners, reinforcement pieces, Arduino board, display, and buttons were supplied or recovered from the Innovation Lab at no direct purchase cost. The final-prototype total also includes RMB 27.00 of miscellaneous retained hardware.

Table 6: Cost of the final vehicle.

Item	Qty.	Cost (RMB)
DC775 high-torque motors	2	138.00
BTS7960 motor drivers	2	32.00
12 V battery and charger	1	107.00
Arduino battery and charger	1	39.80
12 AWG and 13 AWG wires	2 m each	25.60
Journal bearings	4	14.20
15 mm shafts	3	16.00
3D-printed frame and wheels	1 set	0.00
Lab-supplied or recovered hardware	Various	0.00
Miscellaneous retained hardware	Various	27.00
	Total	**399.60**

Table 7: Overall development and testing cost.

Item	Qty.	Cost (RMB)
DC775 high-torque motors	2	138.00
BTS7960 motor drivers	2	32.00
12 V battery and charger	1	107.00
Arduino battery and charger	1	39.80
12 AWG and 13 AWG wires	2 m each	25.60
Worm-wheel and gear sets	2 sets	85.00
40-tooth gears with 8 mm and 15 mm bores	2 each	32.00
Journal bearings	6	14.20
15 mm shafts	3	16.00
10 kg test weights	4	280.00
	Total	**769.60**

The difference of RMB 370.00 between the two totals mainly resulted from parts purchased for concepts that were later changed and from four 10 kg weights purchased for planned load testing. These weights were not used in the documented 75 kg person-carrying test. The difference shows how late design changes increased the total project expenditure even though several purchased components were not included in the final vehicle.

V Testing

Two main tests were carried out on the completed vehicle. The load test was used to evaluate the strength of the PLA frame and the ability of the motors to move a heavy load on a level surface. The gap-crossing test was used to evaluate stability, tread retention, transmission reliability, and the automatic timed-control system under the official challenge conditions.

A Load Test

The vehicle was tested on a flat floor while carrying a person with a mass of approximately 75 kg. Including the vehicle mass of approximately 6 kg, the total moving mass was about 81 kg. The corresponding gravitational load was

$$
\begin{aligned}
W &= mg && (42)\\
&= (81\,\text{kg})\left(9.81\,\text{m/s}^2\right) && (43)\\
&\approx 795\,\text{N}. && (44)
\end{aligned}
$$

The vehicle continued to move forward while carrying this load. No visible bending, cracking, or permanent deformation was observed in the PLA frame or the steel-reinforced legs. This result agreed with the finite element analysis, which predicted a maximum displacement of only 0.097 67 mm under a larger design load of approximately 1000 N.

The two driven axles had a combined rated wheel torque of approximately 12.55 N m. With a wheel radius of 0.025 m, the corresponding ideal circumferential driving force was

$$F_{\text{drive}} = \frac{T_{\text{total}}}{r} = \frac{12.55\,\text{N m}}{0.025\,\text{m}} \approx 502\,\text{N}. \quad (45)$$

The actual force at the ground would have been lower because of transmission losses, belt slip, and rolling resistance. However, the test confirmed that the selected motors and reduction system produced enough torque to move the loaded vehicle on a level surface. It also confirmed that the reinforced frame could support a large static load without noticeable structural damage. This test did not demonstrate that the vehicle could carry the same load across the gap, since it was performed only on a continuous flat surface.

B Gap-Crossing Test

The first gap-crossing tests were carried out using the original six-wheel design. The front and rear wheels were driven, while the centre wheels were initially allowed to rotate freely. Each time the front wheels entered the 200 mm gap, the vehicle tipped forward about the centre-wheel region. The team first suspected that rotation of the centre shaft was causing the problem, so the shaft and centre wheels were rigidly attached to the frame using adhesive and cable ties. This modification did not prevent tipping.

Additional smaller trolley wheels were then added to increase the number of contact points, but they did not provide sufficient support during the critical stage of the crossing. The centre wheels were also replaced temporarily with a wooden block. This arrangement was unsuccessful because the block height did not match the front and rear wheel contact level. Testing eventually showed that the main problem was the loss of support when the front wheels entered the gap. As the front reaction disappeared, the rear wheels unloaded and lifted from the table, leaving the vehicle unable to maintain static equilibrium.

Continuous treads were added as a final modification. The available tread material was not the correct size, so surplus sections were cut and joined using screws to produce sufficient tension around the wheels. The tracks allowed the vehicle to maintain contact with both tables during the crossing, and the modified vehicle successfully crossed the gap in one of two official trials.

The successful trial began behind the official start line, and no one touched the vehicle after the run started. The 200 mm measurement describes the clear gap traversed by the front wheels. The teaching assistant's approximately 6 s stopwatch time covered the complete official run and ended only after the whole vehicle had passed the finish line. Using the 520 mm vehicle length and the two 200 mm start- and end-line offsets gives a minimum travel distance of 1.12 m and a minimum average course speed of approximately 0.187 m/s, as calculated in Eqs. (39) and (40). The vehicle mass during the test was approximately 6 kg. Although one tread began to derail during the successful run, the vehicle still passed completely beyond the end line.

The main failure observed during testing was poor tread and belt retention. The improvised tread joints did not produce uniform tension, so the treads could move sideways and come off the wheels. The toothed transmission belts were also added late in the project and did not include adjustable tensioners. As a result, the belts sometimes loosened or slipped on the motor and shaft pulleys. Uneven power transmission increased the likelihood of the vehicle pulling to one side, which contributed to tread derailment.

No additional payload was successfully carried across the gap because the loose tread and belt systems were not reliable enough. The test nevertheless confirmed that the tracked support concept could cross the 200 mm gap and that the automatic timed-control system could complete the run without human intervention. The most important improvements would be adjustable belt and tread tensioners, lateral tread guides, and more accurately manufactured continuous tracks.

VI Discussion and Recommendations

Testing showed that the main structural and drivetrain calculations were suitable for the intended high-load design. The vehicle moved on a flat surface while supporting a 75 kg person, exceeding the 40 kg minimum payload objective, with no visible cracking or permanent bending of the PLA frame. This agreed with the low displacement predicted by the 1000 N stretch-load simulation. In the official gap-crossing assessment, the vehicle completed one of two trials, giving a 50 % success rate. During the successful trial, the front wheels crossed the 200 mm clear gap and the whole vehicle passed the finish line in approximately 6 s, faster than the 8 s target. The 75 kg load test was carried out only on a flat surface, and no additional payload successfully crossed the gap.

The main weakness was not the frame or motor capacity, but the reliability of the tread and belt systems. The improvised treads were cut and joined to fit the vehicle, which produced uneven tension and allowed them to move sideways during operation. The timing belts also lacked adjustable tensioners and occasionally slipped between the motors and driven shafts. These problems caused inconsistent power transmission and contributed to tread derailment. The final envelope was approximately 520 mm by 310 mm by 180 mm. Relative to the preferred 500 mm by 300 mm plan dimensions, the length was 4.0 % over and the width was 3.3 % over. Because dimensional deductions begin at 5 % over the preferred value in each direction, both dimensions remained within the no-deduction band, while the height remained below the target [1].

If the project were repeated, the drivetrain and crossing mechanism should be finalized earlier so that more time is available for manufacturing and testing. Properly sized continuous treads should be used together with lateral guides to prevent sideways movement. Adjustable tensioners should also be added to both the treads and the motor transmission belts. Further testing should examine each stage of the gap crossing separately, especially the transfer of support from the first table to the second. A longer testing period would allow faults to be identified before the final trial and would reduce the need for last-minute modifications. Clearer task division, regular design reviews, and backup plans for critical components would also improve the reliability of the final prototype.

Acknowledgements

This work was guided by Global College SJTU. The authors express their gratitude to Prof. Bi Youyi and Mr. Otto Zhang for their technical support and for providing the materials necessary for this work. The authors also thank TAs Sihao Peng and Ye Baopu for their timely assistance.

References

[1] VM250 Course Team, "Automatic Gap-Crossing Challenge Environment and Project Requirements," course project brief, Summer 2026.

[2] M. T. Birosz, D. Ledenyák, and M. Andó, "Effect of FDM infill patterns on mechanical properties," *Polymer Testing*, vol. 113, Art. no. 107654, 2022. https://doi.org/10.1016/j.polymertesting.2022.107654

[3] M.-H. Hsueh, C.-J. Lai, C.-F. Chung, S.-H. Wang, W.-C. Huang, C.-Y. Pan, Y.-S. Zeng, and C.-H. Hsieh, "Effect of Printing Parameters on the Tensile Properties of 3D-Printed Polylactic Acid (PLA) Based on Fused Deposition Modeling," *Polymers*, vol. 13, no. 14, Art. no. 2387, 2021. https://doi.org/10.3390/polym13142387

[4] Gates Corporation, *Industrial Power Transmission Product Catalog*, Catalog No. 19993, 2021. https://www.gates.com/content/dam/documents-library/catalogs/power-transmission-catalog.pdf

[5] Arduino, "UNO R3," official hardware documentation. https://docs.arduino.cc/hardware/uno-rev3

[6] Microchip Technology Inc., *ATmega328P: 8-bit AVR Microcontroller with 32K Bytes In-System Programmable Flash*, Datasheet 7810D, 2015. https://ww1.microchip.com/downloads/en/DeviceDoc/Atmel-7810-Automotive-Microcontrollers-ATmega328P_Datasheet.pdf

[7] O. Kraus, "U8g2 Reference Manual," U8g2 project documentation. https://github.com/olikraus/u8g2/wiki/u8g2reference

[8] Infineon Technologies AG, *BTS 7960 High Current PN Half Bridge*, Datasheet Rev. 1.1, Dec. 2004. https://www.infineon.com/dgdl/Infineon-BTS7960-DS-v01_01-en.pdf

[9] Arduino, "Wire Library," official language reference. https://docs.arduino.cc/language-reference/en/functions/communication/wire/

[10] Arduino, "Arduino Language Reference," official documentation. https://docs.arduino.cc/language-reference/

[11] Prusa Polymers, *Prusament PLA Technical Data Sheet*, 2021. https://prusament.com/wp-content/uploads/2022/10/PLA_Prusament_TDS_2021_10_EN.pdf

A Initial Concept Sketches

The following sketches document the concepts considered during the early stages of the project. They include a long multi-wheel chassis, a rack-and-rail bridge, a suction-assisted transfer mechanism, and a tracked vehicle. These concepts were later compared in terms of stability, load capacity, manufacturing difficulty, and crossing reliability.

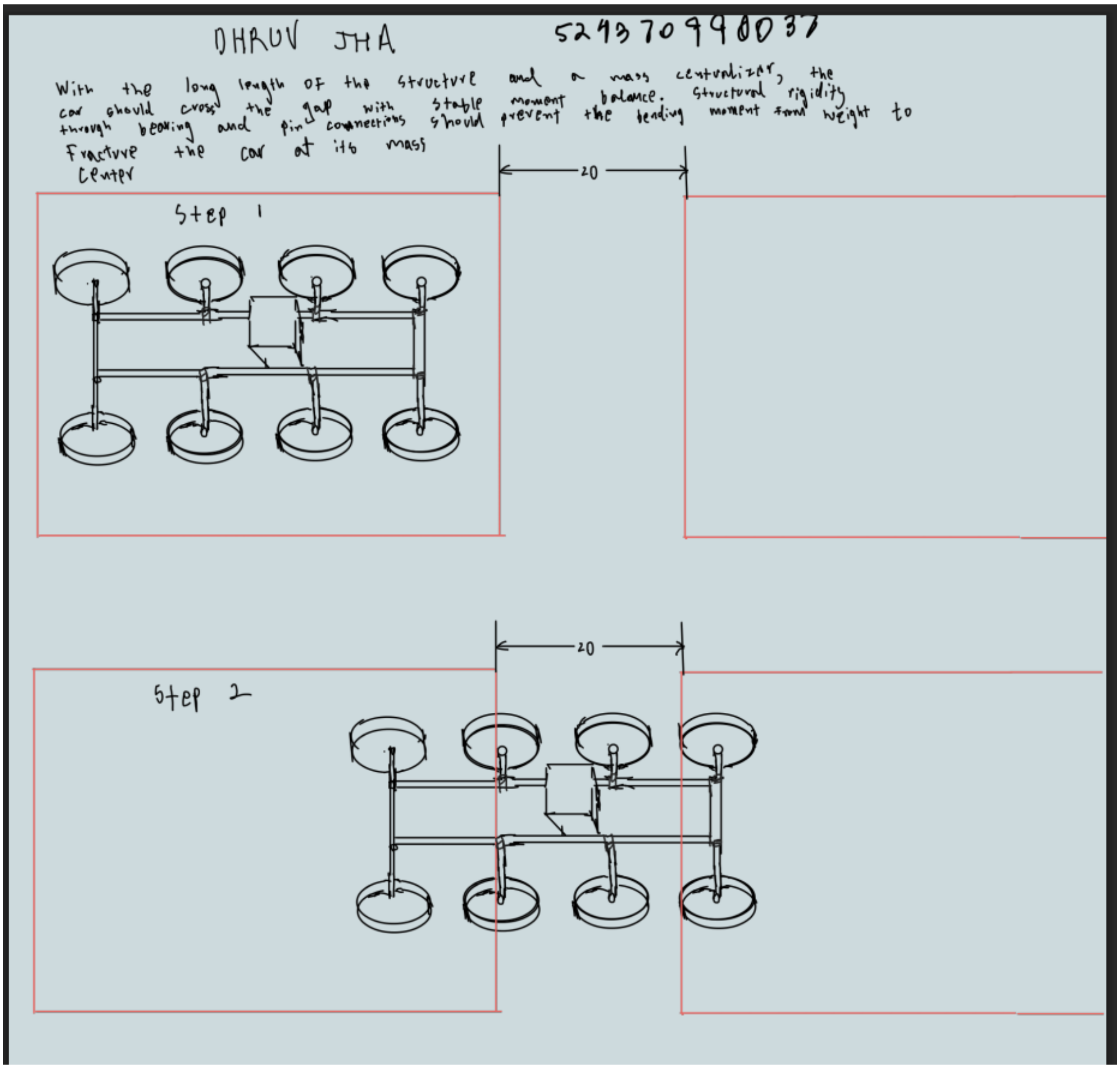

Figure A.1: Long multi-wheel chassis concept by Dhruv Jha, showing the proposed support sequence as the vehicle advances across the 200 mm gap.

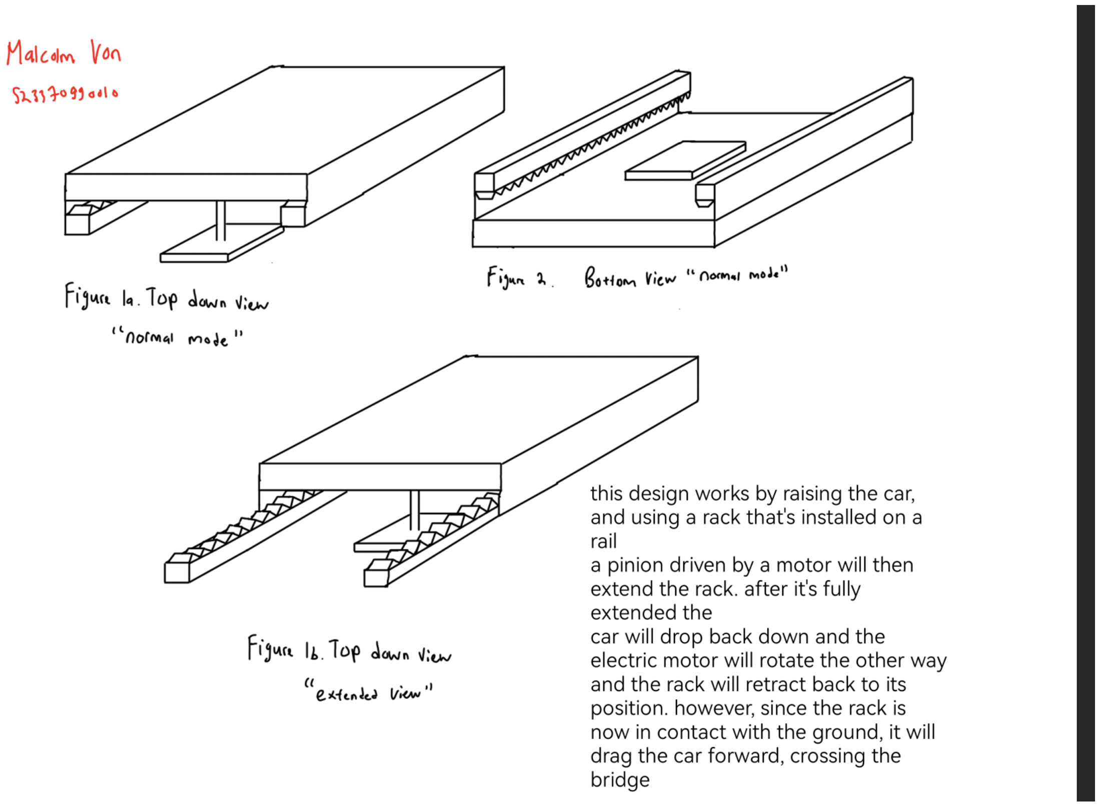

Figure A.2: Rack-and-rail bridge concept by Malcolm Von, showing the normal configuration, the extended rails, and the proposed retraction motion used to pull the vehicle across the gap.

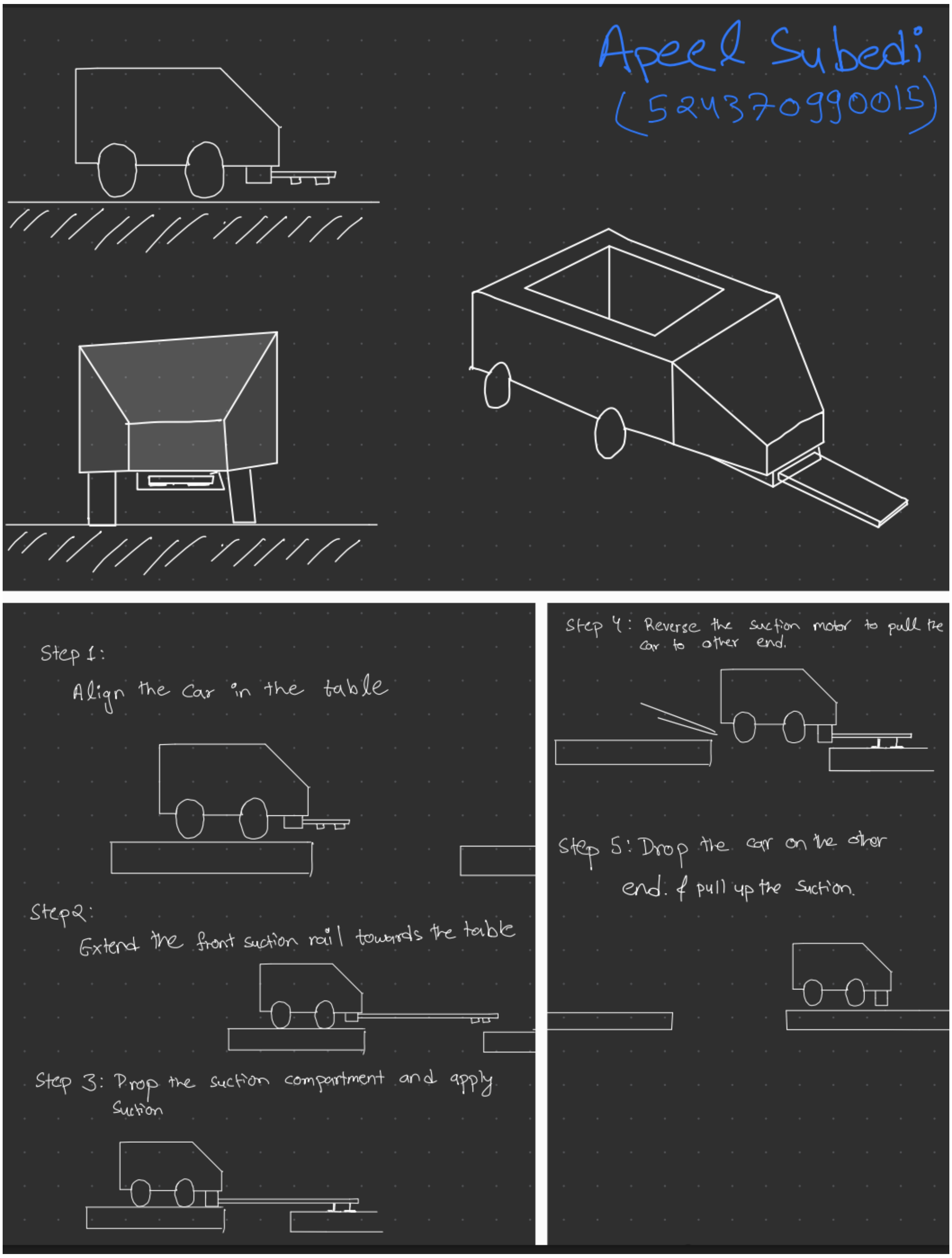

Figure A.3: Suction-assisted transfer concept by Apeel Subedi, showing the extendable front rail, suction attachment, and proposed sequence for securing the vehicle to the far table.

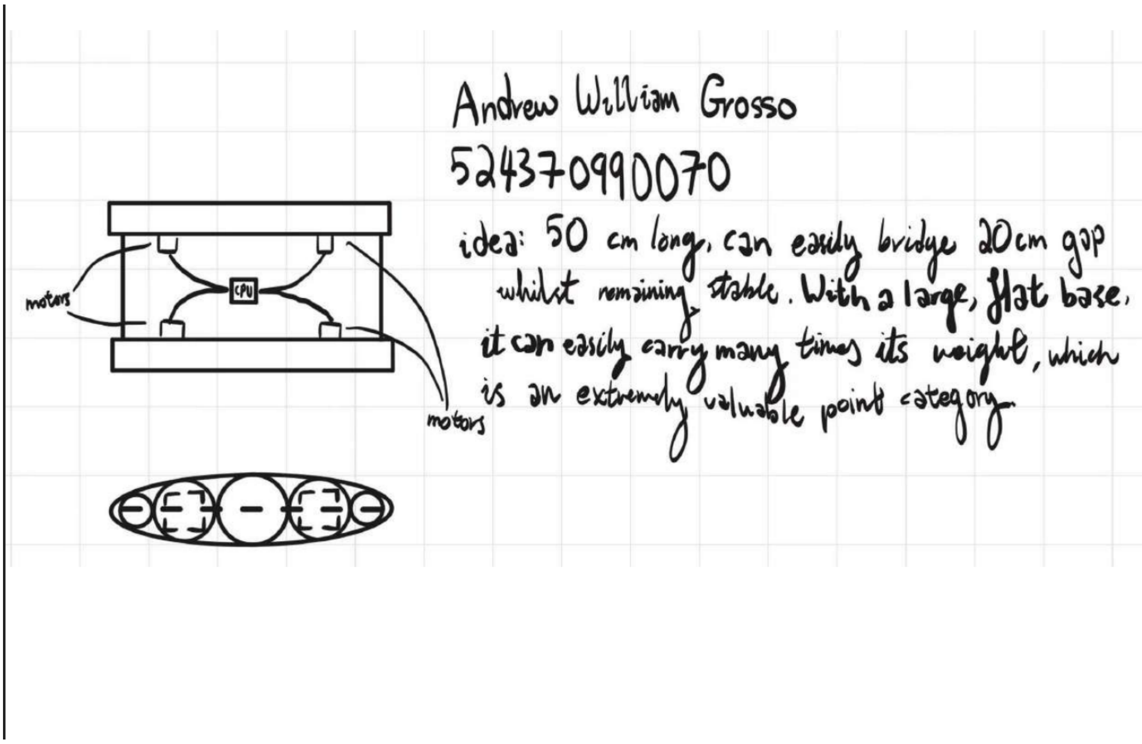

Figure A.4: Tracked vehicle concept by Andrew Grosso, showing a long load-carrying platform, distributed wheel positions, and continuous tracks intended to maintain support across the gap.

B Engineering Drawing

The engineering drawing below presents the principal dimensions and views of the frame assembly used to guide the manufacture and assembly of the vehicle. Unless otherwise stated, all dimensions are in millimetres.

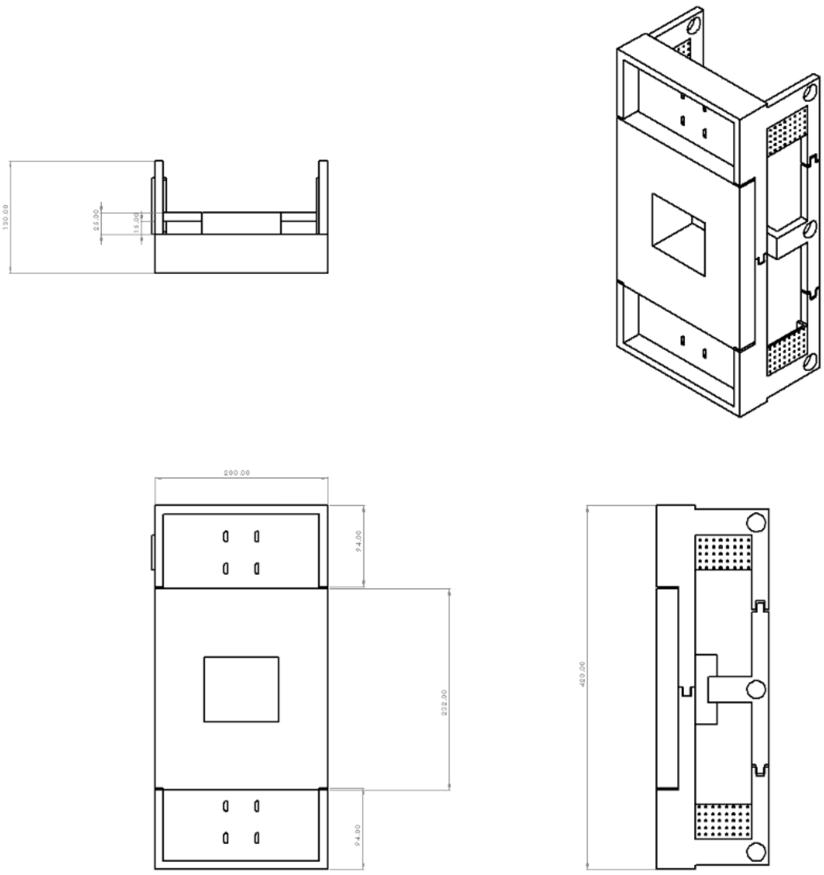

Figure B.1: Dimensioned engineering drawing of the frame assembly, showing the orthographic and isometric views, principal frame dimensions, shaft locations, and component-mounting features.

C Product Design Specification

Table 1: Product design specification and final prototype results.

Design criterion	Target specification	Final result and verification	Status
Gap-crossing capability	Cross a clear gap of at least 200 mm.	The front wheels traversed the measured 200 mm gap during one of the two official trials.	Partially met
Starting position	Begin completely behind the start line located 200 mm before the gap.	The vehicle began behind the official start line during both trials.	Met
Finishing position	The complete vehicle must pass the finish line located 200 mm beyond the gap.	During the successful trial, the whole vehicle passed the finish line.	Met
Automatic operation	Operate without physical assistance after the run begins.	The vehicle used automatic timed control and was not touched after starting.	Met
Crossing time	Complete the official course within approximately 8 s.	The teaching assistant measured approximately 6 s for the complete vehicle to pass the finish line.	Met
Stability during crossing	Remain supported without tipping while transferring between the two tables.	The initial wheel-only design tipped about the middle-wheel region. The tracked design crossed successfully, although the tread partially derailed.	Partially met
Payload capacity	Carry a minimum additional payload of 40 kg on a level surface.	The vehicle moved on a level floor while carrying a person with a mass of approximately 75 kg.	Exceeded
Structural load objective	Evaluate the frame under a maximum desired load of approximately 100 kg.	Finite element analysis used an approximately 1000 N vertical load and predicted a maximum displacement of 0.097 67 mm.	Met analytically
Vehicle envelope	Preferred dimensions of 500 mm by 300 mm by 300 mm.	The final vehicle measured approximately 520 mm by 310 mm by 180 mm. The length and width were within the stated 5 % no-deduction band.	Accepted
Vehicle mass	Keep the unloaded vehicle sufficiently light for the selected motors while maintaining a strong frame.	The vehicle mass during the official crossing was approximately 6 kg.	Met
Wheel size	Use compact wheels compatible with the frame and tread arrangement.	Six printed wheels with a diameter of approximately 50 mm were used.	Met
Propulsion system	Provide sufficient torque to move the vehicle and its intended payload.	Two DC gearmotors drove the front and rear shafts through toothed belt transmissions. The vehicle moved while carrying the	Met

D Control Code

The following listing shows the core firmware used to control the vehicle. The program allows the operator to adjust the motor command while the vehicle is idle, begin the run using the start button, and stop both motors automatically after the programmed crossing time has elapsed.

```
int percentToPwm(int pct) { // Set-point to duty cycle
  if (pct <= 0) return 0;

  int pwm = (MIN_PWM > 0)
            ? map(pct, 1, 100, MIN_PWM, 255)
            : map(pct, 0, 100, 0, 255);

  return constrain(pwm, 0, 255);
}

void loop() {
  if (!running) { // IDLE state
    if (justPressed(bUp) && speedPercent < 100) {
      speedPercent += STEP;
    }

    if (justPressed(bDown) && speedPercent > 0) {
      speedPercent -= STEP;
    }

    speedPercent = constrain(speedPercent, 0, 100);

    if (justPressed(bStart) && speedPercent > 0) {
      running = true;
      runStart = millis();
      driveForward(percentToPwm(speedPercent));
    }

  } else { // RUNNING state
    if (millis() - runStart >= RUN_MS) {
      motorsOff();
      running = false;
    }
  }

  draw();
}
```

Listing 1: Core firmware used for the automatic timed-control sequence.

The control method is open-loop. The selected percentage determines the PWM duty cycle rather than directly measuring the vehicle speed. The command remains fixed during each crossing, and the vehicle returns to the idle state when the programmed run time expires.